Article

Manifestations of Different El Niño Types in the Dynamics of the Extratropical Stratosphere

Tatiana S. Ermakova [1,2,*] , **Andrey V. Koval** [1,2] , **Sergei P. Smyshlyaev** [1,2] , **Ksenia A. Didenko** [1,2] , **Olga G. Aniskina** [1], **Elena N. Savenkova** [1] and **Ekaterina V. Vinokurova** [1]

[1] Meteorological Forecasting Department, Russian State Hydrometeorological University, 192007 Saint-Petersburg, Russia
[2] Atmospheric Physics Department, Saint Petersburg State University, 198504 Saint-Petersburg, Russia
* Correspondence: taalika@mail.ru

Abstract: The behavior of planetary waves and their influence on the global circulation of the Northern Hemisphere during different El Niño types is studied. Three sets of five boreal winters were chosen for each El Niño type: Modoki I and II and canonical El Niño. Based on data of the Japanese 55-year Reanalysis and the Modern-Era Retrospective Analysis for Research and Applications, the spatio-temporal structure of planetary waves and the residual mean circulation were analyzed. The results show that the canonical El Niño type is characterized by the weakest wave activity in March. It is also demonstrated that warming of the polar stratosphere, accompanied by maximizing wave activity and weakening of the zonal wind, may lead to earlier stratospheric polar vortex collapse and the early spring transition under Modoki I conditions. This study is the next step in understanding of the so-called long-range teleconnections, consisting of the propagation of a signal from the tropical El Niño Southern Oscillation source into the polar stratosphere.

Keywords: El Niño; Modoki; planetary waves; wave activity flux; residual meridional circulation; stratospheric dynamics

1. Introduction

El Niño Southern Oscillation (ENSO) has three phases and an irregular cycle of a coupled ocean–atmosphere interaction. It is well known that ENSO plays a crucial role in the formation of extreme weather events in the tropics. A considerable part of the population in tropical regions is familiar with this 'coupled' climate event due to the dangerous weather situations that are observed during the El Niño—the "warm" phase of ENSO. The fish population dies or migrates during El Niño years, since the oceanic upwelling weakens and the coastal ecosystem changes. Increased convection above the warmer surface of the Pacific Ocean brings increased precipitation. This results in heavy rains and devastating floods [1,2]. While South America suffers from floodwaters, severe droughts occur in Indonesia and Australia [3–5].

El Niño and La Niña events interfere with global atmospheric circulation via long-range teleconnections. It has now becomes evident that these naturally occurring phenomena cause weather and climate changes in the extratropics, influencing the propagation of planetary waves (PWs). The movement of atmospheric heat sources to the East leads to uncommon winter conditions at higher altitudes. The observed Sea Surface Temperature (SST) and pressure anomalies can affect even the stratosphere through teleconnections [6–8]. SST via ENSO and equatorial winds through quasi-biennial oscillation impacts the stratospheric waveguide, which influences the vertical propagation of planetary-scale waves from troposphere, resulting in stratospheric polar vortex variability [9,10]. The Aleutian low tends to deepen and shifts southward during El Niño. This leads to the strengthening

of upward wave activity flux into the stratosphere and the weakening of the polar vortex [11–14]. Usually the polar vortex weakens due to a dramatic rise in temperature and pressure in the stratosphere.

The extreme climatic events are caused by an increase of the manifestations of cold outbreaks against the background of observed global warming, which is associated with the less stable stratospheric polar vortex. As a result, arctic air masses penetrate more often into the middle latitudes. On the other hand, an increase of the frequency of cold winters together with a long-term stable stratospheric polar vortex leads not only to the depletion of the ozone layer, but also to a heat decrease and mass exchange between the polar and sub-polar regions and to warm winters.

El Niño is associated with an increase in the number of Sudden Stratospheric Warmings (SSWs) [15]. The SSW is one of the most prominent examples of dynamic interactions between the troposphere and middle layers of the atmosphere. This phenomenon manifests in sharp and significant temperature increases (up to 30–40 K) over the North Pole at altitudes of 30–50 km. The emergence of SSWs is associated with an increase of the propagation of wave activity flux from the troposphere and the nonlinear interaction of PWs with each other and with the stratospheric zonal circulation [16,17] as well as with a sudden displacement (split) of the polar vortex during the reversal/weakening of the stratospheric jet [18,19]. This anomalous situation in the stratosphere affects the tropospheric processes through the negative phase of the Northern Annular Mode or Arctic Oscillation [20,21]. The exact mechanism of the phenomenon that could explain the impact of stratospheric variability on tropospheric circulation is still unclear. However, there are attempts to understand the role of stratospheric and tropospheric wave activity in the time evolution control of downward-propagation anomalies [22–24]. Most studies dedicated to the influence of different phases of ENSO on PWs are based on equatorial-trapped Rossby-Gravity and extratropical planetary waves [25–27], including the stratospheric dynamics [28–31] and ignoring the eastward traveling PWs.

The El Niño phase can be divided into central Pacific (CP or "Modoki"—A Japanese word meaning "similar but different") [32–34] and eastern Pacific (EP or canonical) [15,32,35] according to SST anomaly origin. It is noted that the response of the Aleutian low to the eastern Pacific El Niño type is more substantial and rapid than to the central Pacific [34,36]. The polar stratosphere exhibits more pronounced warming, and the polar vortex weakens during EP as a consequence [37], while there is no consensus on CP, mostly due to differences in its definition.

In order to distinguish two types of El Niño, several methods and indices have been suggested. The El Niño type can be determined by comparing the values of the Niño3 (the Niño3 index measures the equatorial SST anomaly averaged between 150° W and 90° W, 5° S–5° N) and Niño4 (Niño4 is calculated with SSTs in the box 160° E–150° W, 5° S–5° N) indices [38,39]. The SST anomalies in the tropical southeastern Pacific (150°–90° W, 0°–10° S) represent El Niño Modoki events [40]. Some indices are based on the empirical orthogonal function analysis of the SST anomalies [33,41–43].

Based on the opposite impacts on precipitation in southern China during boreal autumn, the El Niño Modoki type was classified into Modoki I and Modoki II [44]. The separation principle includes not only rainfall anomalies but also the spatio–temporal evolutions of SST anomalies. The origin of the positive SST anomaly is located in the equatorial central Pacific and in the subtropical northeastern Pacific during Modoki I and Modoki II, respectively. Wang et al. [45] as shown in Figure 2, reported on the origins and evolutions of SST anomalies for types of El Niño. For El Niño Modoki I, the anomalous warm SST occurs in the tropical central Pacific, while for El Niño Modoki II, it is observed in the subtropical northeastern Pacific. These events further develop in different ways. Hence, the thermodynamic connections of three types of El Niño with the extratropical climate variability may be different and need to be studied.

As it was shown in recent studies [44,46,47], the distributions of precipitation rates differ under conditions of the three El Niño types. Latent heat release, convective cloudiness, and precipitation can influence PWs at stratospheric heights in two ways: explicitly through their additional thermal forcing in the troposphere and implicitly via altering the mean zonal flow, whose distribution determines the propagation conditions of stationary planetary waves (SPWs) (e.g., [48]). It can be assumed that the stratospheric signal in the propagation of PWs will be different due to the different distribution of precipitation during the three types of El Niño. To analyze these signals, the behavior of PWs at different latitudes of 2.5° N, 27.5° N and 62.5° N was examined. Equatorial planetary waves, e.g., the Kelvin wave, are excited by convective heating in the equatorial region [49–51]. A latitude of 27.5° N allows demonstrating the variability of travelling planetary waves, while at higher latitudes, these waves are obfuscated by the standing and quasi-stationary waves [52]. The extratropical low-frequency westward-propagating atmospheric normal modes are well observed at higher latitudes (around 60° N), since their amplitudes are the greatest there (e.g., [53,54]). This paper is dedicated primarily to the studies of the differences in the thermal and dynamic regimes of the atmosphere under Modoki I, Modoki II, and canonical El Niño conditions.

2. Data and Methods

The examination of thermo-dynamic features in the winter stratosphere of the Northern Hemisphere under conditions of different El Niño types has been carried out. The Japanese 55-year Reanalysis (JRA-55) [55] covering the period from 1958 to the present was used for the behavior of PWs under Modoki I, Modoki II, and canonical ENSO conditions analysis.

Using the table of available extended Multivariate ENSO Index (MEI) values (https://psl.noaa.gov/enso/mei.ext/table.ext.html; https://psl.noaa.gov/enso/mei/data/meiv2.data, accessed on 31 March 2022) and results obtained by Wang [45], the following sets of winters were chosen: 1963/64, 1979/80, 1987/88, 1992/93, and 2002/03—corresponding to Modoki I winter conditions (in second column of Table 1, denoted as MI); 1968/69, 1977/78, 1991/92, 1994/95, and 2009/10—Modoki II winters (Table 1—MII); and 1965/66, 1972/73, 1982/83, 1997/98, and 2015/16—canonical El Niño type winters (Table 1—C). Positive values in Table 1 with magnitudes greater than 0.5 (highlighted with bold) indicate the El Niño (warm) phase of the ENSO. The "warmest" winters (with the greatest SST anomaly) are 1972/73, 1982/83, 1997/98, and 2015/16 (canonical type). The "coldest" ones are 1979/80 and 1992/93 (Modoki I type). Winter 1979/80 shows the smallest values of MEI index values; only the late autumn months have magnitudes slightly greater than 0.5. That winter can be referred to as neutral phase, while other ENSO indices (The Oceanic Niño Index (ONI) and Nino3.4) demonstrate positive SST anomaly during winter months; Wang [45] identified that winter as a Modoki I type of El Niño. Positive SST anomaly, according to ONI values, was observed from summer 1991 till summer 1992, and there were values of about 0.7 (threshold of ±0.5) in spring 1993. Therefore, the 1992/93 winter cannot be classified as El Niño winter, taking into account only SST anomaly. The Southern Oscillation Index (SOI) demonstrates negative values for autumn months in 1992 and winter 1992/93. It usually indicates the onset of a warm ENSO phase. The bi-monthly MEI, which includes not only SST but also sea-level pressure, zonal and meridional components of the surface wind, and outgoing longwave radiation, has values of about one unit (threshold of ±0.5). The values of this index were taken as the basis for identifying winters under warm and cold phases of ENSO; thus we consider winter 1992/93 as El Niño.

Table 1. Bimonthly MEI index values. Positive values with magnitudes greater than 0.5 highlighted with bold.

Year	EN Type	JA	AS	SO	ON	ND	DJ	JF	FM	MA
1963/64	MI	**0.91**	**1.06**	**1.11**	**1.07**	**0.97**	**0.93**	**0.73**	0.25	−0.35
1965/66	C	**1.73**	**1.73**	**1.42**	**1.52**	**1.73**	**1.68**	**1.53**	**1.21**	**0.89**
1968/69	MII	−0.34	0.20	**0.62**	**0.73**	**0.66**	**0.76**	**1.04**	**1.03**	**0.94**
1972/73	C	**2.21**	**2.07**	**1.88**	**1.84**	**2.01**	**2.02**	**1.76**	**1.30**	**0.74**
1977/78	MII	**0.75**	**0.72**	**0.83**	**1.01**	**1.11**	**0.94**	**0.85**	**0.90**	**0.57**
1979/80	MI	0.44	0.38	0.24	**0.52**	**0.65**	0.35	0.19	0.41	**0.59**
1982/83	C	**2.02**	**1.81**	**1.93**	**2.28**	**2.48**	**2.57**	**2.74**	**2.68**	**2.79**
1987/88	MI	**1.48**	**1.23**	**1.13**	**0.85**	**0.75**	**0.59**	0.31	0.19	−0.01
1991/92	MII	0.42	**0.62**	**1.09**	**1.17**	**1.29**	**1.70**	**1.59**	**1.72**	**1.98**
1992/93	MI	0.08	**0.50**	**0.81**	**0.73**	**0.78**	**0.83**	**0.93**	**0.78**	**0.98**
1994/95	MII	**0.84**	**1.06**	**1.47**	**0.99**	**0.87**	**0.77**	0.48	0.14	0.18
1997/98	C	**2.20**	**2.17**	**2.01**	**2.06**	**2.03**	**2.23**	**2.43**	**2.27**	**2.55**
2002/03	MI	**0.97**	**0.84**	**0.79**	**0.76**	**0.86**	**0.80**	**0.62**	**0.53**	−0.08
2009/10	MII	**0.52**	0.39	**0.56**	**1.05**	**0.96**	**0.93**	**1.28**	**1.31**	0.49
2015/16	C	**1.92**	**2.21**	**2.11**	**1.88**	**1.90**	**1.94**	**1.81**	**1.31**	**1.33**

In order to analyze amplitudes of PWs, the longitude-time Fourier transform was applied to the geopotential height fields for each of the observed boreal winter periods. The calculated amplitudes of geopotential height variations due to PWs with zonal wavenumbers 1, 2, and 3 are presented in Figure 1 as contours. A strong variability caused primarily by nonlinear interaction of the waves with mean flow (the so-called stratospheric vacillations, e.g., [56,57]) is evident. Another reason of observed variability is the interference of SPWs with travelling waves, for instance, the interference of the SPWs and atmospheric normal modes [53].

To analyze the propagation of PWs in the atmosphere, 3D fluxes of wave activity [58] are considered. The Plumb algorithm makes it possible to estimate the direction of propagation of a wave packet on a three-dimensional plane, which is usually applied to analyze the vertical transition of waves between the stratosphere and the troposphere. Figure 2 shows the calculated three-dimensional flux of wave activity for the winter months during different El Niño conditions.

Analyzing the activity of PWs, it is worth considering its impact on the mean flow. However, in the momentum and energy equations, the wave sources of momentum and heat are compensated by advective momentum and heat fluxes [59]. To fill this gap, the alternative approach was applied, using a calculation of residual mean meridional circulation (RMC) within the transformed Eulerian mean approach (TEM, [60]). RMC is a combination of eddy (generated by waves) and advective mean flows. RMC calculation is widely used as an effective tool for estimating the transport of long-living atmospheric gas species in the meridional plane. The observed variability of RMC can significantly clarify the changes in the thermal regime and ozone content in the Polar Regions during SSW events and/or their dependence on the ENSO, quasi-biennial oscillation (QBO), Madden-Julian oscillation phases, etc. To analyze these changes, the RMC was calculated using MERRA2 (The Modern-Era Retrospective analysis for Research and Applications, [61]) for the years selected to reflect different El Niño types. MERRA2 covers a larger altitudinal range in comparison to JRA-55 (up to 0.1 hPa), which is why it was chosen for RMC calculations. Statistical significance of the results obtained was estimated based on the paired *t*-test.
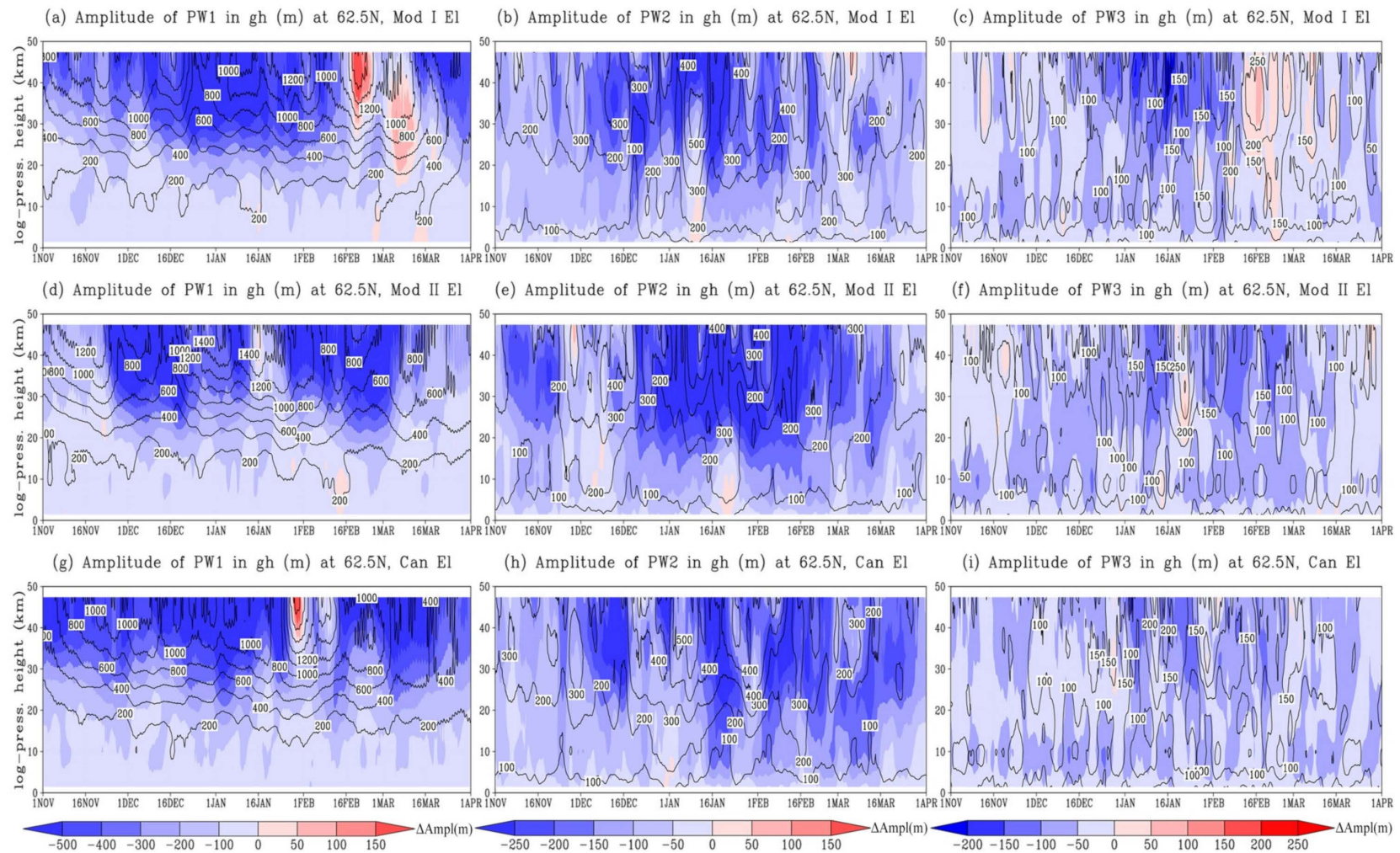
Figure 1. Contours: amplitudes of planetary waves with zonal wavenumber 1 (**left panels**), 2 (**middle panels**), and 3 (**right panels**) in geopotential height (meters) at 62.5° N during Modoki I conditions (**top panels**), Modoki II conditions (**middle panels**), and canonical conditions (**bottom panels**). Shading: respective anomalies relative to climatic distributions (November–March, 1964–2016).

PWs in this study are represented by the standing and travelling components. The traveling planetary waves were extracted using a space–time spectral analysis of the geopotential height fields based on the complex Morlet wavelet transform [62]. It is possible to extract the westward and eastward propagating planetary waves using the phases of geopotential height oscillations obtained at different longitudes. The extraction method was described by [52,63]. In addition to the eastward and westward propagating waves, we consider also the standing waves that arise as a result of the interference of two waves propagating towards each other.
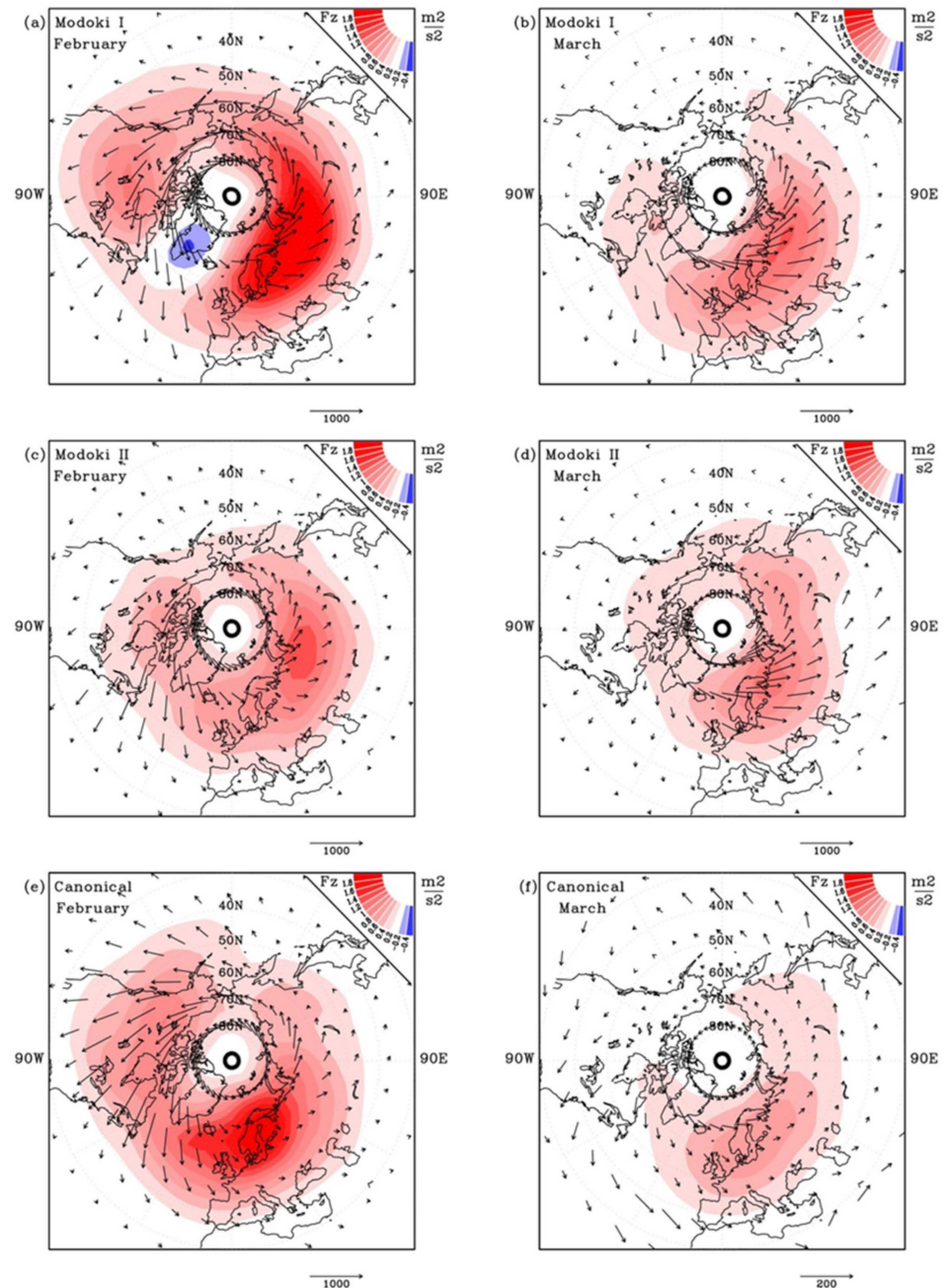
Figure 2. 3D wave activity flux (Fz—shading, [Fx;Fy]—arrows) averaged in February (**left panels**) and in March (**right panels**) at about 40 km during Modoki I conditions (**top panels**), Modoki II conditions (**middle panels**), and canonical conditions (**bottom panels**).

3. Results

For every considered winter, amplitudes of PWs with three wavenumbers were analyzed. For example, the amplitude peaks of PW1 greater than 2500 m arise in January 1964, February 1988, and December 2002 (referred to as Modoki I); in the end of December 1994, December 2009, and January 2010 (Modoki II); in December 1982 and February 2016 (canonical El Niño). In two cases, when the observed peak amplitudes occur in February, the maximum MEI values reach two and appear to be in summer. The substantial PW1 amplitudes in December during both Modoki types can be also related to high MEI values (about one). The top magnitude occurs in early autumn.

The averaged amplitudes of PW1, PW2, and PW3 during different El Niño types are presented with contours in Figure 1. Short time intervals of increased wave activity are found during three types of El Niño in different winter months, but the shortest wave activity period is noticed during the canonical El Niño type. The Modoki II type is distinguished by a calm February and active March, with wave amplitudes of about 1000 m. The amplitudes of waves are much greater in February–March under Modoki I conditions. Similar features can be seen in the behavior of PW1–PW3 amplitudes (Figure 1, panels from left to right).

The planetary wave activity is connected and affects the intensity of the stratospheric polar vortex state. Its extreme state as SSW as well as the final stratospheric warming, which concerns the transition date, is observed in the middle stratosphere. Amplitude differences of PWs under each El Niño type condition and climate are shown in Figure 1 as shading. The values are mostly negative. This confirms that amplitudes of planetary wave are usually greater under La Niña [31] and neutral conditions. The positive anomaly of PW1 (Figure 1a) and PW3 (Figure 1c), which is observed under Modoki I conditions in the end of February and in the beginning of March, can result in more obvious SSW occurrence and the stratospheric polar vortex weakening. If this SSW is considered as final, the early spring transition can be expected. PW2 amplification (Figure 1b) under Modoki I conditions is observed at lower altitudes at about 30 km. It can correlate with the downward wave activity flux that is observed every winter under the conditions of this type. In general, it is clearly seen that in many cases, PW1 and PW 2 are in antiphase: the strengthening of one wave is accompanied by a synchronous weakening of the other. For example, it took place during the peaks of PW 1 on February 18 for Modoki I; on January 2 and 17 for Modoki II; on January 25 for the canonical type. This demonstrates the transfer of wave energy between different wave modes.

Figure 2 shows the horizontal distributions of the vertical component of the 3D wave activity flux (shaded) and its horizontal components (arrows) at an altitude of 40 km for February and March for the three observed El Niño types. Downward flux over Greenland is observed in February during Modoki I type conditions. This type of El Niño is accompanied by the strongest and most extensive wave activity flux during all winter months. This flux is often negligible during canonical El Niño, except in February 2016. Figure 2c demonstrates only upward flux in February under Modoki II conditions, and it is much weaker in comparison with the fluxes during other El Niño types. The weaker wave activity flux during Modoki II conditions corresponds to smaller amplitudes of PW1, PW2, and PW3 in February as shown in Figure 1. Figure 2b shows maximum wave activity in March during Modoki I conditions.

The zonal component of the wave activity flux is directed mainly from west to east, and the meridional component is directed towards the equator. Changes in the horizontal components as a rule correspond to changes in the vertical ones: the areas of intensification of the horizontal flux of wave activity are maximum in February under Modoki I and canonical conditions. The magnitude of the horizontal flux noticeably decreases in March under the canonical El Niño. At Modoki II, a weakening of the zonal 3D flux and an increase of the meridional flux are noticeable in comparison to other types. This effect is observed both in February and March.

Different behavior of the planetary wave activity contributes to the changes in RMC and in thermal conditions of the middle- and high-latitude stratosphere, which are discussed below.

3.1. Changes in Global Atmospheric Circulation during Different El Niño Types

Planetary waves provide wave fluxes of heat and/or long-lived atmospheric species. To account for these fluxes, the residual meridional circulation is considered [60]. Figures 3 and 4 demonstrate monthly mean RMC and zonal wind in February (upper panels) and March (bottom panels) during Modoki II El Niño events (left panels), the difference between canonical and Modoki II (middle panels), and the difference between Modoki I and Modoki II (right panels). The RMC and its increments were considered for different El Niño types for every winter month, but the most interesting results were obtained for February and March. The zonal mean temperature (color shading) in Figure 3 was added for assessment of the thermodynamic situation over the polar region in these months. In February, the Arctic stratosphere is the coldest under Modoki II conditions (Figure 3a) and the warmest during the canonical El Niño type (Figure 3b); the temperature difference may exceed 20 K at 45 km. There is no significant difference in the meridional circulation under Modoki I and Modoki II conditions (Figure 3c), while it is much stronger starting from mid-latitudes toward the North Pole during canonical ones. The enhancement of RMC during the canonical El Niño arises due to increased planetary wave activity in the beginning of February, as shown in Figure 1g. The RMC consists of an *advective* (Eulerian mean) component and *wave-induced* eddy component [64]. The latter increases significantly in the upper stratosphere during the canonical El Niño compared to Modoki II, while the first one weakens. This effect is accompanied by the weakening of zonal circulation under the increased PW activity during the canonical type, as shown in Figure 4b. The enhancement of the northward and downward RMC components in February contributes to the warming of the polar stratosphere shown in Figure 3b. At mesospheric altitudes (55–65 km) during canonical conditions, the opposite behavior is observed: the coldest temperature (about 250 K) occurs as well as the weakening of the meridional flow. In March, the temperature over the North Pole increases and reaches up to 270 K at 55–60 km under Modoki II conditions (Figure 3d). The tendency of the temperature difference as compared with other conditions is similar to the one observed in February, but positive temperature differences between canonical and Modoki II conditions span to the ground (Figure 3e). The maximum wave activity in the stratosphere in March is observed for Modoki I conditions (see Figure 2). This is accompanied by a warming of the mid- and high-latitude stratosphere (Figure 3f), an increase in eddy meridional circulation, a weakening of the advective contribution, as well as a weakening of the polar vortex (Figure 4f). This circumstance may lead to earlier stratospheric polar vortex collapse during Modoki I El Niño events.

The statistical significance of the temperature and zonal wind increments as shown in Figures 3 and 4 was estimated based on the paired *t*-test. Each figure shows the data averaged over three months (one for each observed year, with 3 h output). Statistically insignificant increments areas at the 95% significance level are marked with diagonal hatching. In Figure 3, hatching indicates statistically insignificant data on either temperature or RMC, i.e., statistically significant increments are located only outside the hatching areas.
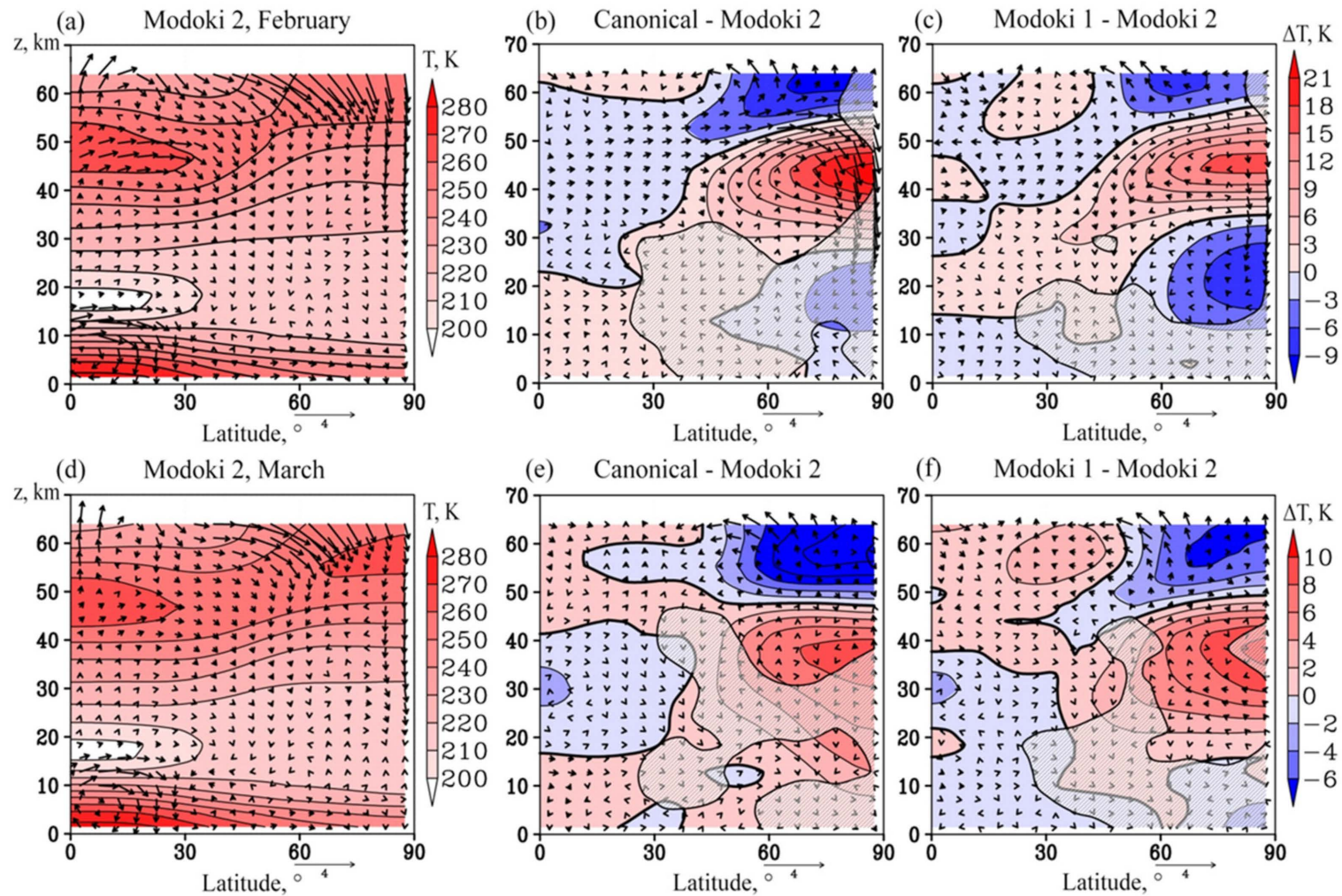
Figure 3. Monthly averaged residual mean meridional circulation (arrows, m/s, vertical component is multiplied by 200) in February (**upper panels**) and March (**bottom panels**) during Modoki II El Niño event (**left panels**); difference between Canonical and Modoki II (**middle panels**); difference between Modoki I and Modoki II (**right panels**). Color shading shows zonal-mean temperature (K). Hatched areas show insignificant temperature and/or RMC increments (at 95%).
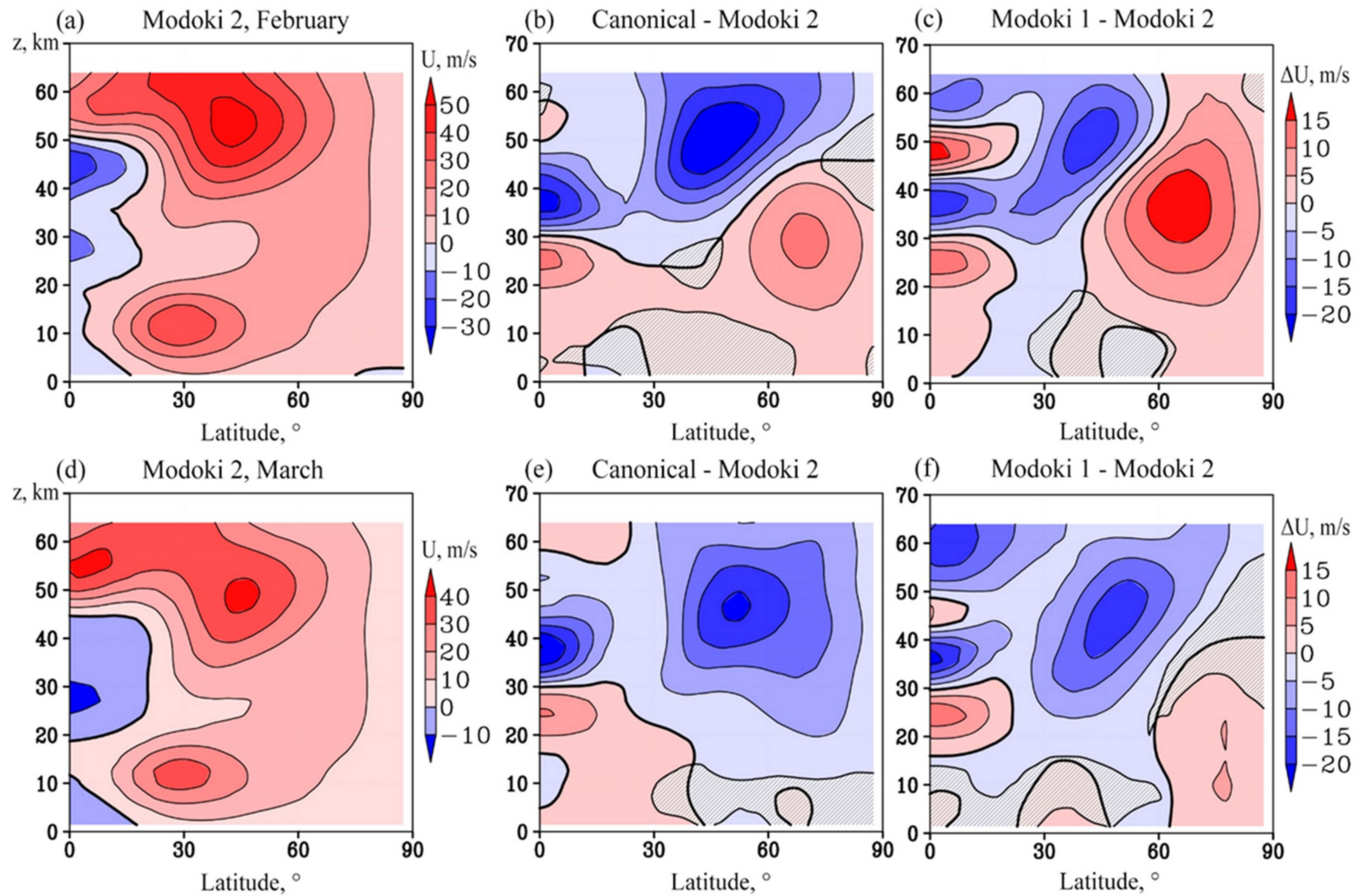
Figure 4. Monthly averaged zonal mean wind (m/s) in February (**a–c**) and March (**d–f**) during Modoki II El Niño event (**a,d**); difference between Canonical and Modoki II (**b,e**); difference between Modoki I and Modoki II (**c,f**).Hatched areas show insignificant data (at 95%).

3.2. Planetary Waves' Structures

As discussed above, the observed temporal variability of the amplitudes of PWs occurs due to the superposition of the variability of PWs, which can be explained by the change in the conditions for their propagation from the troposphere and/or the nonlinear interaction with the mean flow and by the presence of traveling and standing planetary waves. Traveling (eastward and westward propagating) and standing planetary waves, in turn, are also nonstationary. As a result, the situation is rather complicated, and the complex Morlet transform is used to estimate the variability of their amplitudes and phases. The approach of wave division into traveling to the East and West and the further recalculation of the results obtained to distinguish standing waves are described by Pogoreltsev [52].

To assess the separate contribution of different components, the amplitudes of standing PW1 and traveling to the East and to the West PWs were determined at 2.5° N, 27.5° N, and 62.5° N. Despite the different origin of SST anomaly at the equator, some winters have a very similar distribution of both the wave period and maximum amplitude magnitudes. The time distribution of standing PW1 at 62.5° N during all investigated winters is presented in Figure 5 as an example. There is a calm standing wave behavior during winters with Modoki I type (1979/80, 1992/93), Modoki II type (1977/78, 1994/95), and canonical type (1972/73, 1982/83): the most active waves with 3–4 day periods and amplitude peaks do not reach 25 m. Considering traveling waves (not presented), eastward planetary waves with periods greater than 10 days and amplitudes of 2–4 m are observed every winter during Modoki I and canonical types, unlike winters during Modoki II.

Travelling waves determined at 2.5° N latitude during every El Niño type have almost identical wave activity distribution despite the different location of SST anomalies. This allows us to conclude that the SST anomaly is not the only cause of equatorial wave behavior. The standing wave activity at 27.5° N latitude during the Modoki II type is similar to the activity during the canonical type. This similarity disappears at 62.5° N latitude, which is more evident in the figures with the amplitude wave spectra averaged over the cold season. It can be explained by the fact that, commonly, Modoki events are not as strong as canonical ones and are less controlled by equatorial ocean–atmosphere coupling [65].

Traveling planetary waves (normal atmospheric modes, Kelvin waves, etc.), unlike atmospheric tides, do not have permanent sources; therefore, they exist (observed in the results of wavelet analysis) in the form of bursts of wave activity at certain periods that are not associated with a specific time interval [53]. That is why in Figure 5 such a significant temporal and spatial variability of the PW amplitudes is observed. Therefore, to compare the wave activity of traveling planetary waves induced by different types of El Niño events, the amplitude wavelet spectra have been averaged over 5 months (from November to March). Figure 6 demonstrates the standing, eastward, and westward waves averaged over boreal winter seasons during different El Niño types at 2.5° N. These waves were analyzed at 27.5° N and 62.5° N as well. Considering the waves at 2.5° N (Figure 6), it is obvious that both amplitudes of nonmigrating diurnal tide (Figure 6a–c) and amplitudes of Kelvin waves (Figure 6d–f) were overestimated for all years before 1979, regardless of El Niño type, most likely due to the lack of satellite information in the reanalysis data.
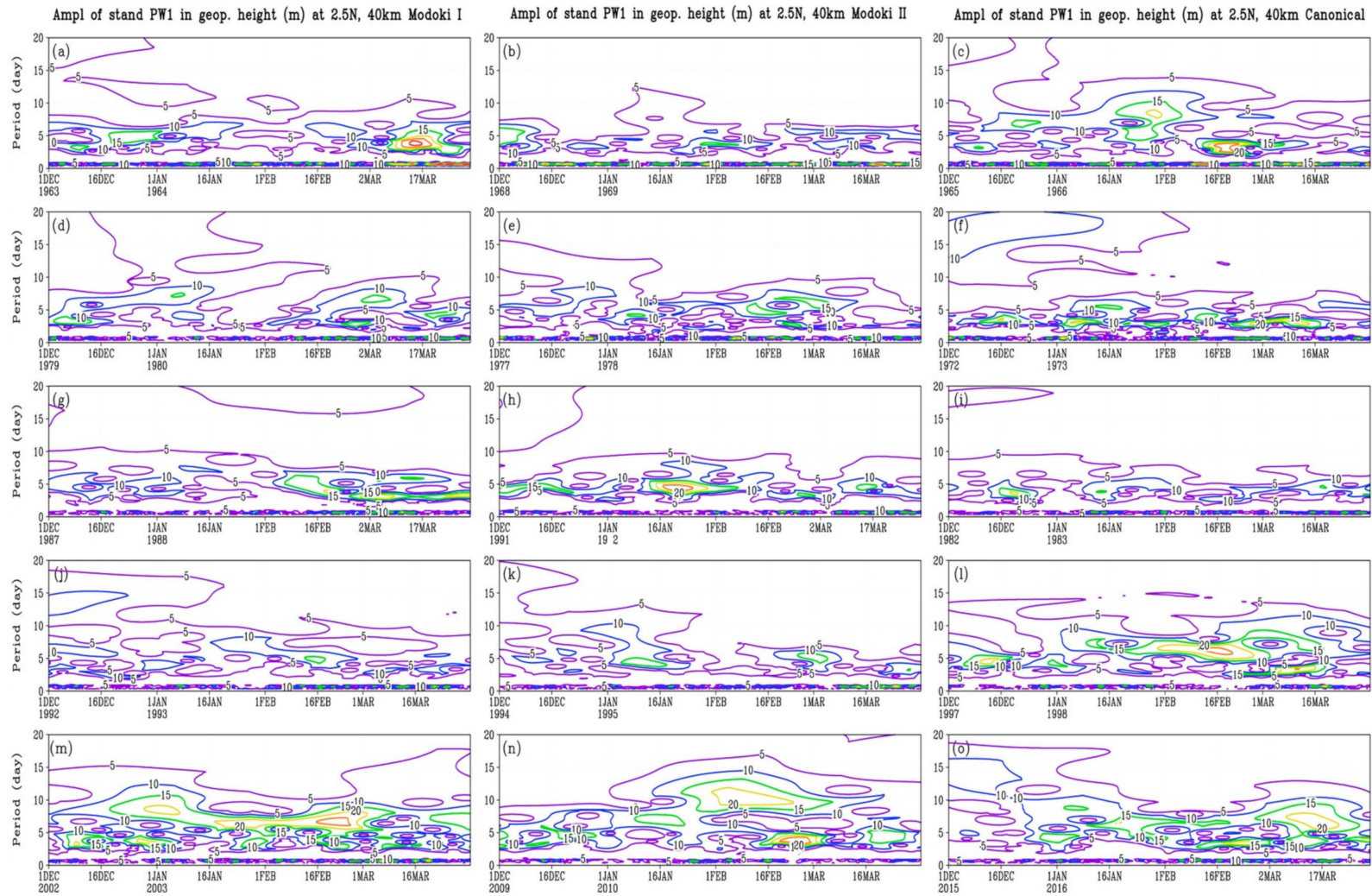
Figure 5. Amplitudes of standing planetary waves with zonal wavenumber 1 in geopotential height (m) at 62.5° N. **Left panels** (**a**,**d**,**g**,**j**,**m**)—winters during Modoki I conditions; **middle panels** (**b**,**e**,**h**,**k**,**n**)—Modoki II conditions; **right panels** (**c**,**f**,**i**,**l**,**o**)—canonical conditions.
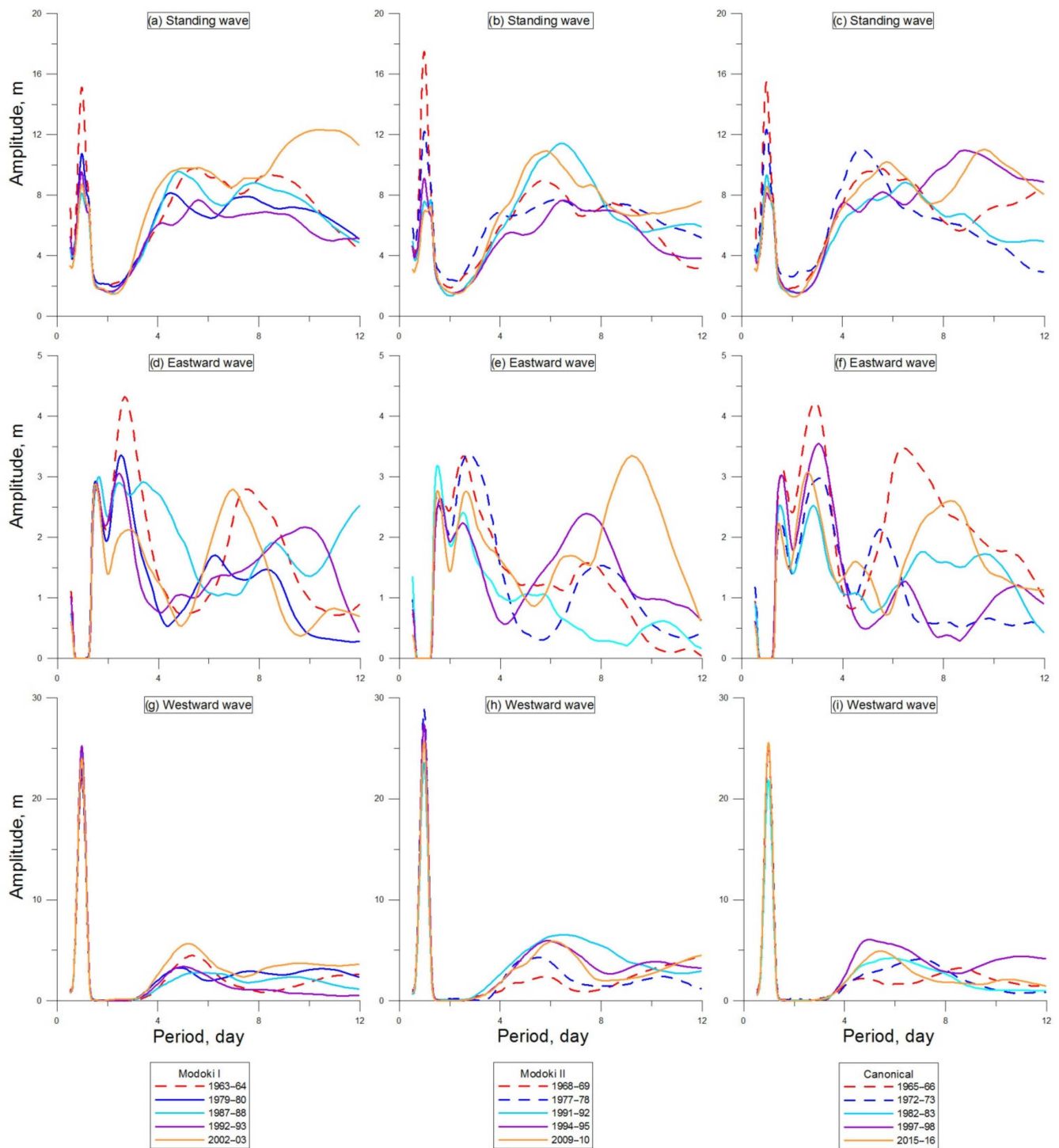
Figure 6. Standing waves (**top panels**), eastward waves (**middle panels**), and westward waves (**bottom panels**) averaged over 5 months (from November to March) during Modoki I (**left**), Modoki II (**middle**), and canonical El Niño (**right**) at 2.5° N. The dashed curves correspond to the wave amplitudes observed in winters before 1979.

It is difficult to estimate the amplitude of the wave spectra averaged over 5 months of the cold season, since the amplitudes of nonmigrating diurnal tides and Kelvin waves are found to be overestimated for all years before 1979. The general shape of curves looks similar, taking into account the maximal amplitudes of standing and traveling waves in

Modoki I and canonical winters. Modoki II differs, with smaller amplitudes and smoother curves. This difference is particularly notable at mid-latitudes, where wave amplitudes are not distinguished from each other every canonical winter, especially standing and westward propagating waves.

There are two peaks of amplitudes over 8 m in Modoki I and canonical events, while there is the only one in Modoki II (see Figure 6a–c). The distribution of eastward propagating waves has no common features in various El Niño types, considering wave amplitudes and periods. The amplitudes of the diurnal migrating tide propagating to the West (Figure 6g–i) are the greatest during Modoki II. It should be noted that this overestimation of diurnal tides is observed in amplitudes at 27.5° N (not presented here) as well, but only in the standing waves, and it is the highest under Modoki II conditions. During this type of El Niño, all westward propagating waves have amplitudes of about 20 m, while in Modoki I and canonical El Niño types, 10 day waves dominate, and the amplitude of about 30 m is observed. The amplitude wavelet spectra averaged over 5 months differ much less during Modoki I and canonical types in contrast to Modoki II at all investigated latitudes, especially for standing and eastward waves.

4. Conclusions

Differences in the thermal and dynamic regimes of the stratosphere associated with different El Niño types were studied. For this purpose, the years reflecting three El Niño types (Modoki I and II and canonical) were selected. The behavior of planetary waves with zonal wavenumbers 1, 2, and 3 in the middle and upper stratosphere during Modoki I and II and canonical El Niño types was considered. The 3 day wave activity fluxes were calculated for all the considered years to interpret the changes in spatio-temporal PW structures.

The strongest upward wave activity flux is located above the two continents of the Northern Hemisphere under Modoki I conditions in all winter months, while the negative wave activity flux over Greenland is observed every February during Modoki I type conditions. During Modoki II conditions, the weak upward flux occupies a much smaller area compared to the fluxes during other El Niño types in February. During canonical conditions, the weakest wave activity flux is located above the middle latitudes of Eurasia, with its maximum over Finland and the Northwest of Russia in March.

In February, the lowest temperature in the Arctic stratosphere is observed under Modoki II conditions, and the highest one is noted during the canonical El Niño type. The meridional circulation under Modoki I and Modoki II conditions is almost identical, while it is much stronger during canonical conditions starting from 40–45° N. In March, the temperature above the North Pole is slightly greater at lower levels of the mesosphere under Modoki II conditions. The tendency of the temperature difference compared with other conditions is similar to the one observed in February, but positive temperature differences between Canonical and Modoki II conditions spread to the ground. During Modoki I conditions, a warming of the mid- and high-latitude stratosphere is observed in March as well as an increase in eddy meridional circulation, caused by enhancement of PW activity flux and a weakening of the polar vortex. These processes may create more favorable conditions for formation of earlier stratospheric polar vortex collapse during Modoki I El Niño events.

Author Contributions: T.S.E. designed the research and performed the analysis. A.V.K. developed software packages for calculating and analyzing the RMC. S.P.S. was involved in the design and interpretation of the results. O.G.A. and K.A.D. provided valuable suggestions for the manuscript. E.N.S. and E.V.V. formed the draft of the manuscript. All authors have read and agreed to the published version of the manuscript.

References

1. Ward, P.J.; Kummu, M.; Lall, U. Flood frequencies and durations and their response to El Niño Southern Oscillation: Global analysis. *J. Hydrol.* **2016**, *539*, 358–378. [CrossRef]
2. Nobre, G.G.; Jongman, B.; Aerts, J.; Ward, P.J. The role of climate variability in extreme floods in Europe. *Environ. Res. Lett.* **2017**, *12*, 084012. [CrossRef]
3. Chung, C.T.Y.; Power, S.B. The non-linear impact of El Niño, La Niña and the Southern Oscillation on seasonal and regional Australian precipitation. *J. South. Hemisph. Earth Syst. Sci.* **2017**, *67*, 25–45. [CrossRef]
4. Iqbal, A.; Hassan, S.A. ENSO and IOD analysis on the occurrence of floods in Pakistan. *Nat. Hazards* **2018**, *91*, 879–890. [CrossRef]
5. Foley, A.; Kelman, I. Precipitation responses to ENSO and IOD in the Maldives: Implications of large-scale modes of climate variability in weather-related preparedness. *Int. J. Disast. Risk Res.* **2020**, *50*, 101726. [CrossRef]
6. Bell, C.J.; Gray, L.J.; Charlton-Perez, A.J.; Joshi, M.M.; Scaife, A.A. Stratospheric Communication of El Niño Teleconnections to European Winter. *J. Clim.* **2009**, *22*, 4083–4096. [CrossRef]
7. Ineson, S.; Scaife, A. The role of the stratosphere in the European climate response to El Niño. *Nat. Geosci.* **2009**, *2*, 32–36. [CrossRef]
8. Rao, J.; Ren, R. A decomposition of ENSO's impacts on the northern winter stratosphere: Competing effect of SST forcing in the tropical Indian Ocean. *Clim. Dyn.* **2016**, *46*, 3689–3707. [CrossRef]
9. Richter, J.H.; Matthes, K.; Calvo, N.; Gray, L.J. Influence of the quasi-biennial oscillation and El Niño–Southern Oscillation on the frequency of sudden stratospheric warmings. *J. Geophys. Res.* **2011**, *116*, D20111. [CrossRef]
10. Lubis, S.W.; Matthes, K.; Omrani, N.-E.; Harnik, N.; Wahl, S. Influence of the Quasi-Biennial Oscillation and Sea Surface Temperature Variability on Downward Wave Coupling in the Northern Hemisphere. *J. Atmos. Sci.* **2016**, *73*, 1943–1965. [CrossRef]
11. Garfinkel, C.I.; Hartmann, D.L. Different ENSO teleconnections and their effects on the stratospheric polar vortex. *J. Geophys. Res.* **2008**, *113*, D18114. [CrossRef]
12. Garfinkel, C.I.; Hartmann, D.L.; Sassi, F. Tropospheric precursors of anomalous northern hemisphere strato-spheric polar vortices. *J. Clim.* **2010**, *23*, 3282–3299. [CrossRef]
13. Smith, K.L.; Fletcher, C.G.; Kushner, P.J. The role of linear interference in the annular mode response to extratropical surface forcing. *J. Clim.* **2010**, *23*, 6036–6050. [CrossRef]
14. Smith, K.L.; Kushner, P.J. Linear interference and the initiation of extratropical stratosphere–troposphere interactions. *J. Geophys. Res.* **2012**, *117*, D13107. [CrossRef]
15. Domeisen, D.I.; Garfinkel, C.I.; Butler, A.H. The teleconnection of El Nino Southern Oscillation to the stratosphere. *Rev. Geophys.* **2019**, *57*, 5–47. [CrossRef]
16. Matsuno, T. A Dynamical Model of the Stratospheric Sudden Warming. *J. Atmos. Sci.* **1971**, *28*, 1479–1494. [CrossRef]
17. Pogoreltsev, A.; Savenkova, E.; Aniskina, O.; Ermakova, T.; Chen, W.; Wei, K. Interannual and intraseasonal variability of stratospheric dynamics and stratosphere-troposphere coupling during northern winter. *J. Atmos. Sol. Terr. Phys.* **2015**, *136*, 187–200. [CrossRef]
18. McInturff, R.M. Stratospheric warmings: Synoptic, dynamic, and general circulation aspects. *NASA Ref. Publ.* **1978**, *1017*, 1–174.
19. McIntyre, M.E. How well do we understand the dynamics of stratospheric warmings. *J. Meteorol. Soc. Japan* **1982**, *60*, 37–64. [CrossRef]
20. Kunz, T.; Greatbatch, R.J. On the Northern Annular Mode Surface Signal Associated with Stratospheric Variability. *J. Atmos. Sci.* **2013**, *70*, 2103–2118. [CrossRef]
21. Wittman, M.A.; Polvani, L.M.; Scott, R.K.; Charlton, A.J. Stratospheric influence on baroclinic lifecycles and its connection to the Arctic Oscillation. *Geophys. Res. Lett.* **2004**, *31*, L16113. [CrossRef]
22. Song, Y.; Robinson, W.A. Dynamical mechanisms for stratospheric influences on the troposphere. *J. Atmos. Sci.* **2004**, *61*, 1711–1725. [CrossRef]
23. Lubis, S.W.; Huang, C.S.; Nakamura, N.; Omrani, N.E.; Jucker, M. Role of Finite-Amplitude Rossby Waves and Nonconservative Processes in Downward Migration of Extratropical Flow Anomalies. *J. Atmos. Sci.* **2018**, *75*, 1385–1401. [CrossRef]

24. Lubis, S.W.; Huang, C.S.Y.; Nakamura, N. Role of Finite-Amplitude Eddies and Mixing in the Life Cycle of Stratospheric Sudden Warmings. *J. Atmos. Sci.* **2018**, *75*, 3987–4003. [CrossRef]
25. Kim, K.-Y.; Kim, Y.Y. Mechanism of Kelvin and Rossby waves during ENSO events. *Meteorol. Atmos. Phys.* **2002**, *81*, 169–189. [CrossRef]
26. Dima, I.M.; Wallace, J.M. Structure of the annual-mean equatorial planetary waves in the ERA-40 reanalyses. *J. At. Sci.* **2007**, *64*, 2862–2880. [CrossRef]
27. Rakhman, S.; Lubis, S.W.; Setiawan, S. Impact of ENSO on seasonal variations of Kelvin Waves and mixed Rossby-Gravity Waves. *IOP Conf. Ser. Earth Environ. Sci.* **2017**, *54*, 012035. [CrossRef]
28. Garcia-Herrera, R.; Calvo, N.; Garcia, R.R.; Giorgietta, M.A. Propagation of ENSO temperature signals into the middle atmosphere: A comparison of two general circulation models and ERA-40 reanalysis data. *J. Geophys. Res.* **2006**, *111*, 6101–6115. [CrossRef]
29. Taguchi, M.; Hartmann, D.L. Increased occurrence of stratospheric sudden warming during El Niño as simulated by WAACM. *J. Clim.* **2006**, *19*, 324–332. [CrossRef]
30. Garfinkel, C.I.; Hartmann, D.L. Effects of the El Niño–Southern Oscillation and the Quasi-Biennial Oscillation on polar temperatures in the stratosphere. *J. Geophys. Res.* **2007**, *112*, D19112. [CrossRef]
31. Ermakova, T.S.; Aniskina, O.G.; Statnaia, I.A.; Motsakov, M.A.; Pogoreltsev, A.P. Simulation of the ENSO influence on the extra-tropical middle atmosphere. *Earth Planets Space* **2019**, *71*, 8. [CrossRef]
32. Larkin, N.K.; Harrison, D.E. On the definition of El Niño and associated seasonal average U.S. weather anomalies. *Geophys. Res. Lett.* **2005**, *32*, L13705. [CrossRef]
33. Ashok, K.; Behera, S.K.; Rao, S.A.; Weng, H.; Yamagata, T. El Niño Modoki and its possible teleconnections. *J. Geophys. Res.* **2007**, *112*, C11007. [CrossRef]
34. Yu, J.-Y.; Kim, S.T. Relationships between extratropical sea level pressure variations and the central Pacific and eastern Pacific types of ENSO. *J. Clim.* **2011**, *24*, 708–720. [CrossRef]
35. Hurwitz, M.M.; Calvo, N.; Garfinkel, C.I.; Butler, A.H.; Ineson, S.; Cagnazzo, C.; Manzini, E.; Peña-Ortiz, C. Extra-tropical atmospheric response to ENSO in the CMIP5 models. *Clim. Dyn.* **2014**, *43*, 3367–3376. [CrossRef]
36. Sung, M.K.; Kim, B.M.; An, S.I. Altered atmospheric responses to Eastern Pacific and Central Pacific El Niños over the North Atlantic region due to stratospheric interference. *Clim. Dyn.* **2014**, *42*, 159–170. [CrossRef]
37. Xie, F.; Li, J.; Tian, W.; Feng, J.; Huo, Y. Signals of El Niño Modoki in the tropical tropopause layer and stratosphere. *Atmos. Chem. Phys.* **2012**, *12*, 5259–5273. [CrossRef]
38. Kug, J.S.; Jin, F.F.; An, S.-I. Two types of El Niño events: Cold tongue El Niño and arm pool El Niño. *J. Clim.* **2009**, *22*, 1499–1515. [CrossRef]
39. Yeh, S.W.; Kug, J.S.; Dewitte, B.; Kwon, M.-H.; Kirtman, B.P.; Jin, F.-F. El Niño in a hanging climate. *Nature* **2009**, *461*, 511–514. [CrossRef]
40. Qu, T.; Yu, J.Y. ENSO indices from sea surface salinity observed by Aquarius and Argo. *J. Oceanogr.* **2014**, *70*, 367–375. [CrossRef]
41. Kao, H.Y.; Yu, J.Y. Contrasting eastern Pacific and central Pacific types of ENSO. *J. Clim.* **2009**, *22*, 615–632. [CrossRef]
42. Di Lorenzo, E.; Cobb, K.M.; Furtado, J.C.; Schneider, N.; Anderson, B.T.; Bracco, A.; Alexander, M.A.; Vimont, D.J. Central Pacific El Niño and decadal climate change in the North Pacific Ocean. *Nat. Geosci.* **2010**, *3*, 762–765. [CrossRef]
43. Takahashi, K.; Montecinos, A.; Goubanova, K.; Dewitte, B. ENSO regimes: Reinterpreting the canonical and Modoki El Niño. *Geophys. Res. Lett.* **2011**, *38*, L10704. [CrossRef]
44. Wang, X.; Wang, C. Classifying El Niño Modoki I and II by different impacts on rainfall in Southern China and typhoon tracks. *J. Clim.* **2013**, *26*, 1322–1338. [CrossRef]
45. Wang, X.; Tan, W.; Wang, C. A new index for identifying different types of El Niño Modoki events. *Clim. Dyn.* **2018**, *50*, 2753–2765. [CrossRef]
46. Weng, H.; Ashok, K.; Behera, S.K.; Rao, S.A.; Yamagata, T. Impacts of recent El Niño Modoki on dry/wet conditions in the Pacific Rim during boreal summer. *Clim. Dyn.* **2007**, *29*, 113–129. [CrossRef]
47. Kim, J.S.; Zhou, W.; Wang, X.; Jain, S. El Niño Modoki and the summer precipitation variability over South Korea: A diagnostic study. *J. Meteorol. Soc. Jpn.* **2012**, *90*, 673–684. [CrossRef]
48. Jacqmin, D.; Lindzen, R.S. The causation and sensitivity of the Northern winter planetary waves. *J. Atmos. Sci.* **1985**, *42*, 724–745. [CrossRef]
49. Chapman, S.; Lindzen, R.S. *Atmospheric Tides: Thermal and Gravitational*; Gordon and Breach: New York, NY, USA, 1970; 200p. [CrossRef]
50. Tsuda, T.; Kato, S. Diurnal non-migrating tides excited by a differential heating due to land-sea distribution. *J. Meteorol. Soc. Jpn.* **1989**, *67*, 43–54. [CrossRef]
51. Forbes, J.M.; Hagan, M.E.; Zhang, X.; Hamilton, K. Upper atmosphere tidal oscillations due to latent heat release in the tropical troposphere. *Ann. Geophys.* **1997**, *15*, 1165–1175. [CrossRef]
52. Pogoreltsev, A.I.; Kanukhina, A.Y.; Suvorova, E.V.; Savenkova, E.N. Variability of planetary waves as a signature of possible climatic changes. *J. Atmos. Sol.-Terr. Phys.* **2009**, *71*, 1529–1539. [CrossRef]
53. Salby, M.L. Survey of Planetary-Scale Traveling Waves: The State of Theory and Observations. *Rev. Geophys.* **1984**, *22*, 209–236. [CrossRef]

54. Fedulina, I.N.; Pogoreltsev, A.I.; Vaughan, G. Seasonal, interannual and short-term variability of planetary waves in Met Office stratospheric assimilated fields. *Quart. J. R. Met. Soc.* **2004**, *130*, 2445–2458. [CrossRef]

55. Kobayashi, S.; Ota, Y.; Harada, Y.; Ebita, A.; Moriya, M.; Onoda, H.; Onogi, K.; Kamahori, H.; Kobayashi, C.; Endo, H.; et al. The JRA-55 Reanalysis: General specifications and basic characteristics. *J. Meteor. Soc. Jpn.* **2015**, *93*, 5–48. [CrossRef]

56. Holton, J.R.; Mass, C. Stratospheric Vacillation Cycles. *J. Atmos. Sci.* **1976**, *33*, 2218–2225. [CrossRef]

57. Pogoreltsev, A.I.; Vlasov, A.A.; Fröhlich, K.; Jacobi, C. Planetary waves in coupling the lower and upper atmosphere. *J. Atmos. Sol.-Terr. Phys.* **2007**, *69*, 2083–2101. [CrossRef]

58. Plumb, R. On the Three-Dimensional Propagation of Stationary Waves. *J. Atmos. Sci.* **1985**, *42*, 217–229. [CrossRef]

59. Charney, J.G.; Drazin, P.G. Propagation of planetary-scale disturbances from the lower into the upper atmosphere. *J. Geophys. Res.* **1961**, *66*, 83–109. [CrossRef]

60. Andrews, D.G.; McIntyre, M.E. Planetary waves in horizontal and vertical shear: The generalized Eliassen–Palm relation and the mean zonal acceleration. *J. Atmos. Sci.* **1976**, *33*, 2031–2048. [CrossRef]

61. Gelaro, R.; McCarty, W.; Suárez, M.J.; Todling, R.; Molod, A.; Takacs, L.; Randles, C.; Darmenov, A.; Bosilovich, M.; Reichle, R.; et al. The Modern-Era Retrospective Analysis for Research and Applications, Version 2 (MERRA-2). *J. Clim.* **2017**, *30*, 5419–5454. [CrossRef]

62. Torrence, C.; Compo, G.P. A Practical Guide to Wavelet Analysis. *Bull. Am. Meteorol. Soc.* **1998**, *79*, 61–78. [CrossRef]

63. Pogoreltsev, A.I.; Fedulina, I.N.; Mitchell, N.J.; Muller, H.G.; Luo, Y.; Meek, C.E.; Manson, A.H. Global free oscillations of the atmosphere and secondary planetary waves in the MLT region during August/September time conditions. *J. Geophys. Res.* **2002**, *107*., ACL 24-1–ACL 24-12 [CrossRef]

64. Koval, A.V.; Chen, W.; Didenko, K.A.; Ermakova, T.S.; Gavrilov, N.M.; Pogoreltsev, A.I.; Toptunova, O.N.; Wei, K.; Yarusova, A.N.; Zarubin, A.S. Modelling the residual mean meridional circulation at different stages of sudden stratospheric warming events. *Ann. Geophys.* **2021**, *39*, 357–368. [CrossRef]

65. Capotondi, A.; Wittenberg, A.T.; Newman, M.; Di Lorenzo, E.; Yu, J.-Y.; Braconnot, P.; Cole, J.; Dewitte, B.; Giese, B.; Guilyardi, E.; et al. Understanding ENSO Diversity. *Bull. Am. Meteor. Soc.* **2015**, *96*, 921–938. [CrossRef]